Advanced Materials Technologies

ADVANCED MATERIALS TECHNOLOGIES
www.advmattechnol.com

RESEARCH ARTICLE OPEN ACCESS

Development of Laterally Graded X-Ray Multilayer Optics

Arindam Majhi[1] | Wadwan Singhapong[1,2] | Wai Jue Tan[1] | Andrey Sokolov[3] | Stefano Agrestini[1] | Mirian Garcia-Fernandez[1] | Kejin Zhou[1] | Andrew C. Walters[1] | Chris Bowen[2] | Alexander J.G. Lunt[2] | Hongchang Wang[1] | Kawal J. Sawhney[1]

[1]Diamond Light Source, Harwell Science and Innovation Campus, Didcot, Oxfordshire, UK | [2]Centre For Integrated Materials, Processes & Structures (IMPS), Department of Mechanical Engineering, University of Bath, Bath, UK | [3]Helmholtz-Zentrum Berlin für Materialien und Energie, BESSY-II, Berlin, Germany

Correspondence: Hongchang Wang (hongchang.wang@diamond.ac.uk)

Received: 26 June 2025 | **Revised:** 28 November 2025 | **Accepted:** 29 November 2025

Keywords: laterally graded multilayers | mask optimization | polarizers | sagittal thickness uniformity | X-ray reflectivity

ABSTRACT

Laterally graded multilayer optics play an important role in advanced X-ray applications, enabling precise control of beam properties for spectroscopic and focusing techniques. The Multilayer Deposition System (MDS) at Diamond Light Source (DLS) has demonstrated its ability to fabricate highly precise laterally graded X-ray optics. Developing such optics is challenging due to stringent requirements for precise lateral thickness variations and sagittal uniformity, achieved through optimized substrate speed profiles and advanced mask design. This study presents a comprehensive investigation into the design, fabrication, and characterization of laterally graded multilayers. An adjustable mask design improves sagittal uniformity and reduces optimization times. The structural and optical performance of the multilayers is evaluated, confirming their suitability for synchrotron applications. Two types of laterally graded multilayers were developed: one with a constant lateral gradient (0.005 nm/mm) for O-K edge polarizers, achieving sagittal thickness variations of approximately 0.3–0.4% across an 80 mm substrate, and another featuring a strong variable gradient from 0.037 to 0.112 nm/mm, designed to match the elliptical periodicity profile. The constant gradient multilayer polarizer has been successfully implemented on the state-of-the-art I21 beamline at DLS, highlighting the MDS's role in producing next-generation X-ray optics that meet the stringent demands of synchrotron beamlines.

1 | Introduction

Multilayer optics [1–4] are extensively used in synchrotron radiation instrumentation, including micro-probes [5], spectrometers [6, 7], monochromators [8], and polarimeters [9]. In magnetron sputtering, by modulating the process parameters such as substrate motion, target power distribution, and masking techniques, multilayers with lateral or depth-graded profiles can be fabricated, which is essential for applications such as variable-period Bragg reflectors [10, 11] and supermirrors [12, 13].

Laterally graded multilayers, where the periodicity varies along the substrate length, are typically used in synchrotron applications that require tunable optical properties [9, 14–16]. These multilayer structures are typically deposited on three primary substrate geometries, namely (i) flat, (ii) parabolic, and (iii) elliptical, which are fabricated for the specific application [17]. The nature of the gradient in periodicity can be designed as either constant or variable, and is aligned with substrate geometry. For example, as a focusing device, the multilayer-based Kirkpatrick-Baez (K-B) mirror consists of two elliptical cylindrical mirrors—either bent or polished—that are arranged orthogonally and coated with laterally graded multilayers with variable gradient that accommodate the variation in grazing incidence angles across the mirror surface [15, 18]. The multilayer K-B system enhances the numerical aperture and improves diffraction-limited spatial resolution despite a narrow energy bandpass of a few percent; it can maintain achromatic focusing over a range of photon energies [19].

Polarimeters, in particular those operating in the extreme ultraviolet (EUV) and soft X-ray regions, face significant challenges when crystal-based designs are employed due to their high absorption and refractive index, close to unity [9]. Hence, multilayers have been considered as effective alternatives, offering an improved signal-to-noise ratio. Their performance can be tailored across a broad wavelength range by optimizing the material combinations and periodicity. In polarization studies, periodic multilayers are often used at quasi-Brewster angles owing to their interference structures [20–23]. However, their narrow spectral bandwidth limits their usage in broadband spectrum applications.

To address these needs, laterally graded multilayers with a constant gradient have attracted interest for use in polarimeters as analyzers and phase retarders [7, 9, 24, 25]. This capability is necessary for advanced experimental measurements, such as Resonant Inelastic X-ray Scattering (RIXS), X-ray Magnetic Circular Dichroism (XMCD), and X-ray Linear Dichroism (XLD) [7]. Despite their advantages, the fabrication of laterally graded multilayers is particularly challenging due to the requirement for sub-nanometer precision in the layer thickness across the substrate. For example, the I21 beamline at Diamond Light Source (DLS), which is specialized for soft X-ray RIXS, requires sophisticated optical elements to meet its high-performance criteria [26]. A key requirement for the beamline upgrade is the development of a laterally graded multilayer polarizer with periodicity varying from 3.36 nm to 3.65 nm with a constant gradient of 0.005 nm/mm as well as a sagittal uniformity below 1% for operating at O-K edge (∼530 eV). Therefore, the challenges lie in not only achieving sub-nanometer precision in layer thickness but also maintaining the sagittal uniformity across a large substrate, typically in the range of 100×100 mm^2.

Achieving this high level of precision over a large area necessitates advanced deposition systems and innovative design strategies. To mitigate these challenges, the recently commissioned multilayer deposition system (MDS) at DLS enables dynamic deposition, where the substrates are precisely translated across the sputtering target [4]. This system allows the periodicity gradient to be controlled through the translation speed. In addition, to achieve a uniform thickness distribution along the sagittal direction, a shadow mask technique is employed. The shadow mask is typically placed between the sputtering target and the substrate, selectively blocking the sputtered atoms. The aperture of the shadow mask is optimized based on the geometry of the sputtering system, the shape of the target, and the source profile. Various aperture types, such as parabolic [27, 28], circular [1], multi-Gaussian [29], multi-aperture [30, 31], have demonstrated the potential to achieve an improved uniformity of less than 1.0%. However, detailed studies in mask optimization are limited and, to date, most have focused on planetary rotation magnetron sputtering systems [29, 31, 32], proving limited insight into the optimization process for linear deposition systems.

This paper presents the development of W/B_4C laterally graded multilayers with both constant and variable gradient, fabricated on a flat substrate using the MDS at DLS. The design, fabrication, and characterization of the multilayer optics are discussed, highlighting the challenges of achieving lateral gradients through an optimized speed profile and ensuring sagittal uniformity using novel adjustable shadow masks. This mask design not only enhances the sagittal uniformity but also reduces the time taken during optimization. Furthermore, the parameters of the multilayer structure and optical performance of the multilayer are evaluated in detail, demonstrating its suitability for synchrotron applications. A specific case is demonstrated in which a constant gradient laterally graded multilayer functions as a multilayer polarizer for a soft X-ray RIXS beamline. In addition, this paper presents the development of an advanced variable-gradient multilayer, with a strong lateral gradient from 0.037 to 0.112 nm/mm.

2 | Theory and Experimental

2.1 | Laterally Graded Multilayer Design and PID Parameter Optimization

Generally, laterally graded multilayers are fabricated on three types of substrate geometries—flat, parabolic, and elliptical—depending on the intended application. Flat multilayers are primarily used as monochromators, where a multilayer period across the surface is critical for wavelength selection, while curved multilayers, such as parabolic or elliptical designs, are ideal for focusing optics to efficiently converge the X-ray beams. Figure 1 illustrates two typical configurations: a flat substrate (Figure 1a) and an elliptical substrate (Figure 1b). The flat mirror configuration is described mathematically by the equation:

$$sin^2\theta = \frac{t^2}{l^2} \tag{1}$$

Where θ is the grazing angle, t is the offset position in the reflection plane, and l is the local distance from the X-ray interaction point to the focus (for a converging beam), as reported by [17]. The solid and dashed lines represent reflections from two different positions of the mirror along the gradient corresponding to two different multilayer periods for a particular incident photon energy. In contrast, the elliptical mirror configuration is described by the Equation (2)

$$sin^2\theta = \frac{b}{pq} \tag{2}$$

Where b is the semi-minor axis of the ellipse, p is the distance from the source to the impact point of the optics, and q is the distance impact point of the mirror and the focus.

To achieve the desired lateral gradient of the bilayer thickness, the formula for different geometries must be applied to the Bragg Equation:

$$2dsin\theta\sqrt{1 - \frac{2\delta}{sin^2\theta}} = m\lambda \tag{3}$$

Here, d is the bilayer period, θ is the grazing angle, δ represents the real part of the refractive index, λ is the wavelength, and m denotes the diffraction order.

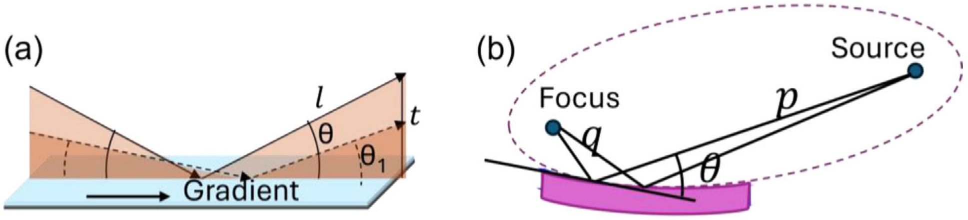

FIGURE 1 | Reflection geometry of the grazing angle optics using laterally graded multilayer structure in (a) flat contour, where the solid and dashed lines represent reflections from two different positions along the multilayer gradient and (b) elliptical contour.

The multilayer deposition is performed using a technique known as dynamic deposition, in which the substrate is continuously translated along the horizontal (meridional) direction in front of the sputtering source. This movement is carefully controlled at a precisely calibrated speed. By adjusting the translation speed in synchronization with the deposition rates, it is possible to accurately tailor the thickness profile of the multilayers, enabling the fabrication of laterally graded or uniform multilayer structures depending on the application requirements.

The translation speed of the substrate plays a critical role, particularly during the deposition of laterally graded multilayers, as it directly influences the achieved periodicity gradient across the lateral direction. The speed profile is designed to control the deposition time at each point on the sample, enabling precise thickness adjustments and creating a lateral gradient in the multilayer stack. The speed profile of the deposition is calculated as follows:

$$T(x) = \int \frac{f(y-x)}{V(y)} dy \tag{4}$$

where $T(x)$ is the expected thickness, $V(y)$ is the speed profile of the moving substrate, and $f(y-x)$ is a source deposition profile. To calculate the speed profile that yields the desired thickness, it is started with an initial speed profile and used an iterative method to find the error in thickness by comparing it to the targeted value. Then $V(y)$ is adjusted to ensure that the simulated thickness matches the targeted thickness profile.

The thickness error is defined by:

$$\delta T(x) = T_{expected}(x) - T_{simulated}(x) \tag{5}$$

Equation (4) can be written as:

$$T_i = \sum_j \frac{f_{ij}}{V_j} \Delta y \tag{6}$$

Using this approach, the following expression can be derived, which describes the change V, given $\delta T(x)$, leading to the Jacobian matrix K

$$\delta T \approx K \cdot \delta V \tag{7}$$

Where,

$$K_{ij} = \frac{\partial T(x_i)}{\partial V(y_j)} \approx -\frac{f(y_j - x_i)}{V(y_j)^2} \cdot \Delta y \tag{8}$$

By substituting Equation (5) into Equation (7), the least-squares method can be used to calculate δV, and update $V + \alpha\delta V \rightarrow V$, where $\alpha \leq 1$ is chosen to prevent large, noisy jumps. However, sometimes the matrix K can be ill posed, and produces large oscillations in V, giving an unrealistic speed profile. To prevent that, Equation (7) can be modified to

$$\begin{bmatrix} K \\ \beta D \end{bmatrix} \cdot \delta V = \begin{bmatrix} \delta T \\ 0 \end{bmatrix} \tag{9}$$

Where,

$$D = \begin{bmatrix} 1 & -1 & 0 & \dots & 0 \\ 0 & 1 & -1 & \dots & 0 \\ \vdots & \vdots & \ddots & \ddots & \vdots \\ 0 & 0 & \dots & 1 & -1 \\ 0 & 0 & \dots & 0 & 1 \end{bmatrix}, \ \beta \in [0, 1] \tag{10}$$

which can be solved using the least-squares method:

$$\min_{\delta V} \left(\|K \cdot \delta V - \delta T\|^2 + \beta^2 \|D \cdot \delta V\|^2 \right)$$

This process is repeated until the thickness deviation (δT) is reduced to approximately 0.2% or lower, which was used as the target tolerance in this work.

The substrate translation speed during deposition determines the periodicity gradient in laterally graded multilayers. Consequently, achieving precise substrate motion requires advanced control strategies that maintain consistent speed profiles throughout deposition. The speed variations directly affect layer thickness and periodicity, making robust speed control critical for high-quality multilayer structures. Using standard commercial software for motion control possibly resulted in discrete speed-step adjustments. To overcome this limitation, the motion speed control was integrated into the Diamond light source standard motion control system, enabling a continuous and precisely defined speed profile. This advancement not only allows very stringent specifications to be met but also provides precise control of non-linear thickness profiles. However, optimal PID (Proportional-Integral-Derivative) parameter tuning is essential to achieve the desired balance between speed accuracy, stability, and dynamic performance [33]. These parameters, namely—Proportional (KP), Integral (KI), and Derivative (KD) gains—collectively determine how the system reacts to deviations from a desired motion profile, thereby influencing both the position accuracy and the overall dynamic behavior. Specifically, the proportional gain (KP) makes the system respond faster to errors but can cause overshooting, while also reducing steady-state error.

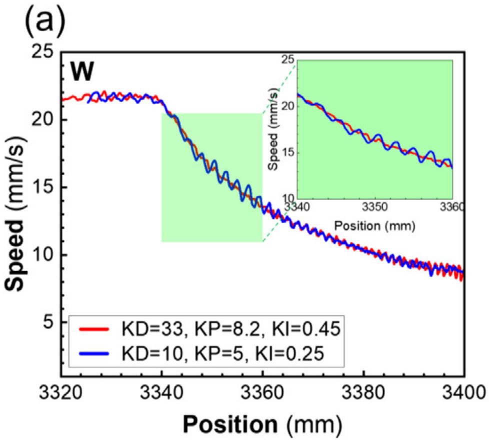

FIGURE 2 | Speed profile during the deposition of the W and B_4C layer, showing the effect of two different sets of PID parameters: KD = 33, KP = 8.2, KI = 0.45 (red curve) and KD = 10, KP = 5, KI = 0.25 blue curve. The optimized set red curve achieves improved speed stability, with speed accuracy refined to approximately 0.1%.

The derivative gain (KD) predicts future errors by responding to the rate of error change, thereby reducing overshoot and enhancing stability, but does not affect steady-state error. The integral gain (KI) eliminates steady-state error by accumulating past errors and continuously adjusting until the error reaches zero. However, excessive KI can slow down the system and induce oscillation. Together, these three parameters must be carefully balanced: KP for quick response, KI for accuracy, and KD for stability.

The PID parameters were tuned manually step-by-step following the Galil velocity zone tuning approach. First, the Galil-Tools-scope was set up to display commanded and actual velocity, position error, and torque, while a step-response DMC (Digital Motion Controller) program was prepared to move the motor sufficiently to overcome static friction and achieve steady velocity. The initial gains were set to KP = 0, KI = 0, and KD = 10, after which the step response was executed to compare commanded and actual velocity profiles. The KD gradually increased until the actual velocity matched the commanded profile. Once the velocity terms were optimized, the KP was introduced, starting from 5 and increased stepwise to reduce position error, with position error reset at each stage for safety. The KI was added with a small starting value to remove steady-state errors, while the integrator limit (IL) was tuned to suppress oscillations. Through iterative refinement of KP, KI, and KD, with continuous monitoring of the torque trace to avoid amplifier saturation, the final tuned values ensured stable and accurate tracking of the commanded motion profile. Fine-tuning these values allows the system to maintain high-speed accuracy—typically within 0.1%—across a wide operational speed range (5 to 50 mm/s), while also reducing settling time and enhancing system stability. Figure 2 illustrates how variations in these PID parameters influence the speed profile during the deposition of the W and B_4C layer in a laterally graded W/B_4C multilayer structure with a variable gradient. Experimental optimization of the PID controller led to the values KD = 33, KP = 8.2, and KI = 0.45, which significantly reduced speed fluctuations compared with the default setting (KD = 10, KP = 5, KI = 0.25) and ensured reliable performance with speed accuracy maintained within 0.1%, as highlighted in the inset figure. In Figure 2a,b, the two optimized speed profiles result underscore the importance of precise PID tuning in delivering consistent and high-quality thin film deposition in multilayer fabrication processes.

2.2 | Multilayer Deposition and Characterization

The W/B_4C laterally graded multilayers were fabricated using the magnetron sputtering system at DLS [4]. The lateral thickness gradients were achieved by controlling the translation speed profile of the substrate, while sagittal profiles were adjusted using custom masks. The base pressure achieved ~2.3×10^{-8} mbar during deposition. A few sets of multilayer coatings were deposited to optimize the period uniformity along the sagittal direction, and at the optimized mask condition, the W/B_4C laterally graded multilayer has been deposited. The deposition power of W and B_4C were 100 and 400 W, respectively. The optimized deposition rates of W and B_4C are 0.1368 and 0.1748 nm/s, respectively. For the working gas mixture, 90% high-purity argon (99.99%) was combined with 10% nitrogen (N_2). This reactive sputtering environment was carefully selected to effectively reduce the interface roughness, enhancing the optical performance of the multilayer [34]. The multilayers were deposited at a fixed working gas pressure of 3.1×10^{-3} mbar.

The parameters of multilayer structure were measured using hard X-ray reflectivity (XRR) with a Bruker D8 Discover X-ray diffractometer at an energy 8.047 keV. Measurements were conducted with a 1 mm vertical slit and a 1 mm pinhole slit on the incident beam and a 2.5×2.5 mm^2 slit on the reflected beam, employing θ-2θ geometry for the XRR analysis. To characterize multilayer periodicity variations along the gradient direction, XRR measurements were performed at sequential positions along the sample's central line spanning a 58 mm range. Additionally, sagittal uniformity was assessed by conducting XRR measurements at consecutive positions across the sagittal direction over a 78 mm range of the multilayer sample. During the shadow mask optimization process (detailed in Section 2.3), the thickness of individual W and B_4C layers deposited on Si substrates was measured along the sagittal direction relative to the sample's center position across an 80 mm span. The measured XRR curves were fitted using the "IMD" code under the "XOP" software package [35] and Genx software [36].

Complementing the structural characterization, the optical performance of the multilayers was evaluated using synchrotron radiation to assess their reflectivity behavior under actual operating conditions. The soft X-ray reflectivity performance of the laterally graded multilayer was characterized using an 11-axis UHV reflectometer at the Optics beamline of BESSY-II [37]. Reflectivity measurements were conducted through a θ-2θ angular scan at an energy of 1000 eV in s-polarization geometry, as well as a continuous energy scan at a fixed incident angle of $2\theta = 20°$ in both s- and p-polarization geometries, covering the energy range near the O-K edge (~530 eV).

The energy scan was performed at six positions along the lateral gradient over a 29 mm range, centered at the middle of the mirror, and at seven positions along the sagittal direction over a 30 mm range. The cross-section of the incident beam at the sample position is 0.35×0.25 mm^2. The beam spot size on the sample is proportional to the beam cross-section, but in the in-plane dimension it is stretched over by factor of $1/\sin(\theta)$, while off-plane size is kept the same. Thus, for energy scans at an incident angle of 20° in the s-polarization geometry, the beam spot was 1.02×0.25 mm^2. The beam angular divergence was $d\theta = 0.03°$, and the energy divergence was 0.23 and 0.6 eV (at 560 and 1000 eV, respectively). The spectral purity of the incident beam was ensured by an efficient high-order suppression system (HiOS) at the Optics beamline [38]. The measured reflectivity curves were analyzed using the IMD code within the "XOP" software package [35].

Beyond this characterization, the fabricated multilayers were also tested in the intended application environment to validate their practical performance. In the polarimetric RIXS apparatus of I21 beamline, the fabricated W/B_4C laterally graded multilayer has been installed vertically perpendicular to the scattering plane, positioned at a grazing incidence angle of 20° relative to the incoming X-ray beam. This configuration is illustrated in Figure 3. For detection, the setup includes two Andor Ikon L CCD detectors: one positioned to record the direct RIXS signal, and another to capture the signal reflected by the multilayer, enabling polarization-resolved detection. The spatial resolution of both CCD detectors needs to match each other for a proper analysis of the RIXS scattered signal: hence, the two detectors, identical with the same pixel size, are mounted with the same tilting angle so that the scattered X-ray beam arrives on both detector sensors with the same incidence angle of 20°.

2.3 | Mask Design and Optimization

The MDS features eight rectangular sources (dimensions W × L = 254 × 89.9 mm), designed to provide a uniform flux at the central region. The aperture size is rectangular of dimension 245 × 82 mm. The translational motion of the substrate within the sputtering chamber is restricted to the lateral direction to maintain thickness uniformity in that axis. Achieving lateral period uniformity has been demonstrated, with a deviation of only 0.26% over a 1500 mm range in dynamic deposition mode [4]. However, it is crucial to also investigate the thickness distribution along the sagittal direction. Our observations indicate that the sagittal thickness uniformity deviates, forming a parabolic profile. This variation is influenced by the dimensions of the sputtering source and the sputtering yield distribution.

As a result, the goal of the mask design is to cut out a section of the total area that provides a non-uniform thickness distribution along the sagittal direction. Accordingly, the shadow masks have been designed in a hyperbolic shape with a sagittal depth, R as shown in Figure 4. The length (L) is set to 220 mm. Given that mask optimization is a time-consuming and iterative process, the mask has been designed to be adjustable by modifying the opening distance (D). This adjustment controls the opening width (W) through which the plasma passes to deposit material on the surface [39]. Consequently, deposition is repeated with different opening distances until the desired uniformity thickness profile is achieved.

To refine the control of mask size and shape, two sets of W and B_4C single layers were deposited on 90 × 25 mm^2 silicon substrates, using a constant lateral translation speed. For B_4C deposition with the mask applied, a 1.3 nm W binding layer was introduced to enhance the contrast between the B_4C film and the Si substate, thereby improving Kiessig fringe visibility for more accurate data analysis. The coating thickness was measured using the XRR technique to evaluate uniformity along the sagittal direction of the substrate. The outcomes of these experiments are discussed in the following sections. The X-ray reflectivity (XRR) plot in Figure 5a shows reflectivity versus incident angle (theta) for a B_4C film measured at different sagittal positions ranging from −40 mm to +40 mm, with and without a mask. The curves measured at different sagittal positions (−40 to +40 mm) with the mask overlapping almost perfectly, demonstrating excellent lateral uniformity. Figure 5b shows the normalized thickness of the B_4C film along the sagittal direction, comparing single-layer film deposited without the shadow mask and with the mask under varying distances of D. The result indicates that without the shadow mask (red line), the thickness of the B_4C at the edge of the sample is significantly lower than at the center, confirming a parabolic distribution with higher sputtering yield at the center. A thickness variation of a maximum 6% was observed from the center toward the edges over an 80 mm range, exceeding the desired tolerance of less than 1% over the same length. This behavior is characteristic of the magnetron source profile, as also observed in previous studies [1, 28]. The thickness distribution curve is fitted using the parabolic equation:

$$y = ax^2 + bx + c \tag{11}$$

where the coefficient "a" is the quadratic coefficient, which represents the curvature of the curve. "b" is the linear coefficient and "c" is the constant coefficient. We aim to bring "a" term as close to zero as possible to flatten the thickness distribution curve, hence improving the thickness uniformity.

The masks were initially configured with an R value of 20 mm. At a fully open setting (D = 40 mm), the deposited film exhibits the lowest thickness at the center of the sample, with a thickness variation of 5%, indicating an overcorrection in the deposition rate. Then, R was reduced to 15 mm, which is determined to be the optimal sagittal depth. Figure 5b shows that varying the mask

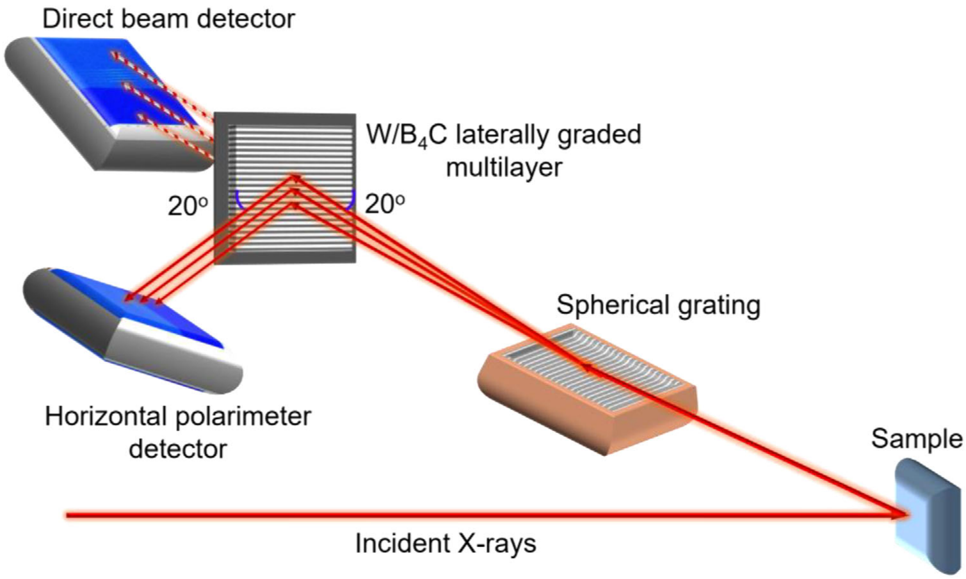

FIGURE 3 | Schematic of the direct beam and polarimeter setups in I21 at Diamond Light Source. The polarimeter configuration features two Andor Ikon L CCD detectors;—one for measuring the direct RIXS signal and another positioned to detect the beam reflected by the multilayer analyzer. Here, the fabricated W/B_4C laterally graded multilayer polarizer optic for operating at O-K edge (~530 eV) has been installed vertically.

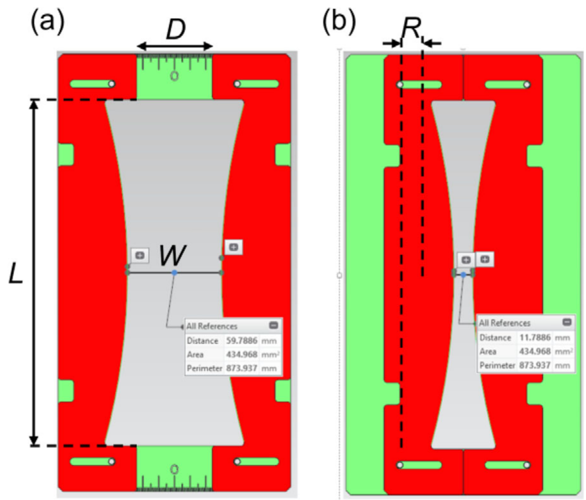

FIGURE 4 | Schematic of the shadow mask, where R represents the sagittal depth of the arc of the mask. The opening distance (D) is adjustable during the optimization process, allowing control over the open area with the width (W) that the plasma particles can pass through. The length of the mask (L) is set to 220 mm for all designs. The red areas indicate the adjustable mask arms mounted on the green rectangular frame, while the gray region represents the opening through which atoms can pass. Figures (a) and (b) show different views corresponding to the maximum and minimum openings of the mask.

opening distance from 50 mm to 20 mm causes the uniformity distribution curve to shift from a downward to an upward orientation, indicating a transition of the quadratic coefficient from negative to positive values. Figure 5c plots the D of the mask against the measured quadratic coefficient. The y-intercept of the linear regression identifies the optimal mask opening distance for achieving good sagittal thickness uniformity. The optimal D is determined to be 32 mm for W and 43 mm for B_4C. Figure 5d presents sagittal thickness of B_4C thin film corresponding to different thickness (d) values (16 mm, 113 mm, and 146 mm) with associated uniformity ($\Delta d/d$) of 0.3%, 0.5%, and 0.6%, respectively, demonstrating excellent spatial uniformity across the measurement range of 80 mm. Following implementation of the optimized mask opening, the thickness profile showed significant improvement with excellent uniformity $\Delta d/d < 1\%$ which met the beamline requirements and further confirmed the reproducibility and precision of the deposition system under different operational parameters. This refinement demonstrates the effectiveness of the optimized mask in controlling layer deposition for laterally graded multilayers.

3 | Results and Discussion

3.1 | Structural Analysis of Laterally Graded Multilayer Using XRR

A W/B_4C laterally graded multilayer polarizer optics for operating at the O-K edge (~530 eV) on flat contour Si substrate geometry has been designed. The fixed operational incidence angle is at 20°. To meet these requirements, we manufactured a W/B_4C laterally graded multilayer on Si substrate with a full dimensional profile of (L × W) of 58 × 78 mm. The W/B_4C multilayer is selected for its high reflectivity in X-ray scattering applications and excellent interface quality. Tungsten (W) provides strong X-ray contrast, while boron carbide (B_4C) serves as a low-density spacer, minimizing interfacial roughness and diffusion. This combination enhances optical performance, making it well-suited for precision X-ray optics [40]. To optimize the reflectivity performance, it is chosen that the Γ ratio of the multilayer is 0.29 to ensure that the W layer thickness is continuous layer [40–42] and the number of layer pairs has been optimized at 100. The designed period thickness ranging from 3.36 to 3.65 nm, with a thickness constant gradient of 0.005 nm/mm, ensures a high

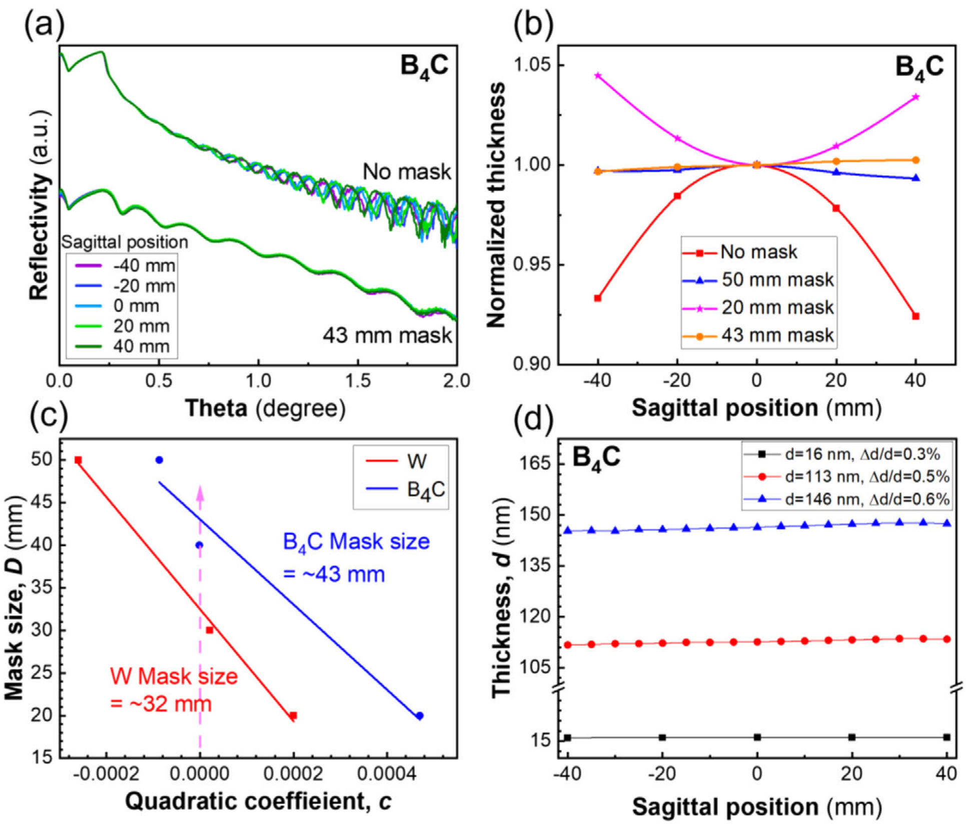

FIGURE 5 | (a) Sagittal uniformity measurement of B_4C thin film using XRR measurements at varying sagittal positions with and without mask. (b) Normalized thickness profile of B_4C single layer deposited on Si substrate along the sagittal direction over 80 mm. The profile compares the film deposited without a mask and with a shadow mask of a 15 mm sagittal depth under varying mask opening distances. (c) Linear regression plot of the mask opening distance versus the quadratic coefficient used to optimize mask width. The optimized mask opening distances, D, are 32 and 43 mm for W and B_4C targets, respectively. (d) Sagittal uniformity of B_4C thin films with a 43 mm mask opening over an 80 mm range for 3 different thicknesses of 16, 113, and 146 nm. Thickness uniformity of better than 0.6% was achieved across all conditions.

precision. The uniformity along the width is maintained at below 1%, optimizing the overall coating performance.

The deposition process ensures a highly precise thickness gradient in the multilayer structure, allowing for variations in thickness and composition that are fine-tuned across the surface to meet the optical and energy requirements of the beamline. This meticulous fabrication approach supports advanced synchrotron radiation experiments, enhancing reflectivity and efficiency at the designated energy levels.

The discussion of the experimental results is highlighted in Figure 6. The XRR measurements were taken at 13 positions along the 58 mm meridional range and 14 positions along the 78 mm sagittal range to confirm these results. Figure 6a shows the lateral periodicity variation across a 58 mm range, illustrating the successful design and fabrication of the laterally graded multilayer, which compares the calculated and measured periodicity profiles. The results exhibit a strong correlation, affirming the precision of the fabrication process with a measured gradient of 0.0052 nm/mm. This verification emphasizes the efficacy of the multilayer deposition in achieving targeted lateral gradient. Figure 6b shows the periodicity deviation with respect to the calculated profile where the maximum deviation is measured to be ~0.2%.

As presented in Figure 6c, the measured and fitted XRR profile at 8.047 keV provides insight into the multilayer's structural parameters at the center position, revealing a W layer density of 19.0 gm/cm^3 (98.4% of the bulk value) and a B_4C layer density of 2.52 gm/cm^3, alongside an average interface roughness of 0.29 nm and a gamma ratio of approximately 0.31 as well as the period thickness 3.50 nm. Figure 6d highlights the uniformity in period thickness across the sagittal direction, showing that a high degree of uniformity (0.3%) was maintained over an 80 mm length, meeting stringent specifications for beamline optics. The comprehensive results, including the meticulous structural parameter measurements, highlight the capabilities of the newly installed MDS at DLS for advanced multilayer optic production.

3.2 | Soft X-Ray Optical Performance

The fabricated W/B_4C laterally graded multilayer is specifically designed for precise soft X-ray manipulation near the oxygen K-edge (~530 eV), requiring detailed structural characterization to evaluate its performance for soft X-ray spectroscopy applications in this critical energy range. The measured reflectivity performance is illustrated in Figure 7, obtained from measurements at the BESSY-II Optics beamline. Figure 7a presents the measured

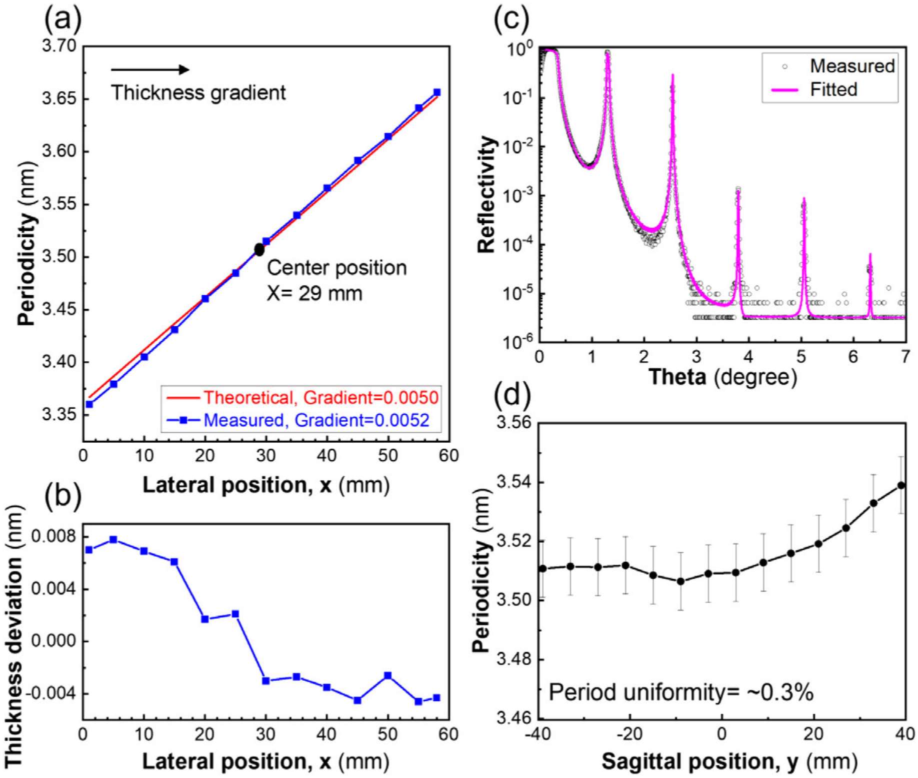

FIGURE 6 | (a) Calculated and measured periodicity along gradient direction over 58 mm. Calculated thickness gradient is 0.005 nm/mm and the gradient of the measured periodicity is 0.0052 nm/mm. (b) Periodicity deviation with respect to the calculated profile. Maximum deviation is measured to be ~0.2%. (c) Measured XRR data and fitted profiles at the center position along the lateral direction at an energy of 8.047 keV; indicated by black circle in (a). (d) Periodicity along the sagittal direction over 80 mm. Uniformity is ~0.3 % along the sagittal direction.

and fitted reflectivity performance at 1000 eV with s-polarized light at the center of the mirror. The reflectivity profile clearly demonstrates well-defined Bragg peaks up to the 4th order, confirming the multilayer's ability to produce high-quality diffraction patterns. Structural parameters are extracted by fitting both the Bragg peaks and the critical angle, yielding precise values for the multilayer's period thickness, density of the layers, and roughness of the interfaces. These parameters show a strong agreement with those obtained from hard X-ray reflectivity measurements. The best-fit results indicate a period thickness of 3.51 nm and a gamma ratio of 0.31, suggesting a well-controlled layer structure. The densities of the individual layers were determined to be approximately 19.0 g/cm^3 for W (98.4% of the bulk value) and 2.52 g/cm^3 for B_4C. The average interfacial roughness is 0.28 nm. The strong agreement between the two measurement techniques confirms that the multilayers were fabricated with a consistent and well-controlled interface quality across all 100-layer pairs, from top to bottom. The small peak-like features observed between the 2nd and 4th Bragg peaks may arise from instrumental artifacts (higher-order harmonic contamination) from the beamline plane grating monochromator. Furthermore, the reflectivity curve exhibits a slight modulation between the critical angle and the first Bragg peak, suggesting the presence of a contaminated top layer. This contamination is most likely due to the formation of B_2O_3 (boron oxide) on the surface [43, 44], as indicated by the observed modulation in the reflectivity data. The oxide layer is estimated to have a thickness of approximately 3.4 nm, a density of 2.35 g/cm^3 (95% of bulk density), and a roughness of 1.6 nm.

Figure 7b presents the reflectivity performance along the sagittal direction, demonstrating a high degree of uniformity over a 29 mm span. This stability is essential for maintaining consistent optical performance across the entire multilayer surface. The reflectivity remains steady at approximately 10.8% over this range, while the fitted periodicity remains uniform at 3.51 nm. The consistency of both the reflectivity data and periodicity confirms that the multilayer structure maintains its uniformity across a broad area, highlighting the success of the fabrication and deposition process.

Figure 7c,d display the reflectivity performance along the gradient, with measurements taken using s-polarized (Figure 7c) and p-polarized (Figure 7d) X-rays. The reflectivity of the multilayer when illuminated with s-polarized light is approximately 10.8%, while for p-polarized light, it is approximately 6.5%. These measurements highlight the polarization-dependent performance of the multilayer, which is a key consideration in its application, especially in precision soft X-ray optics. The difference in reflectivity between s- and p-polarized light emphasizes the multilayer's ability to manipulate the polarization of the incident X-rays, an essential feature for many spectroscopy applications.

To validate the soft X-ray reflectivity performance characterized at BESSY-II and investigate the multilayer's performance for its intended application, the multilayer was further tested at the I21 beamline of DLS as a polarimeter supporting the RIXS experiment. The fabricated W/B_4C multilayer polarizer has been tested by measuring the signal of the photons elastically

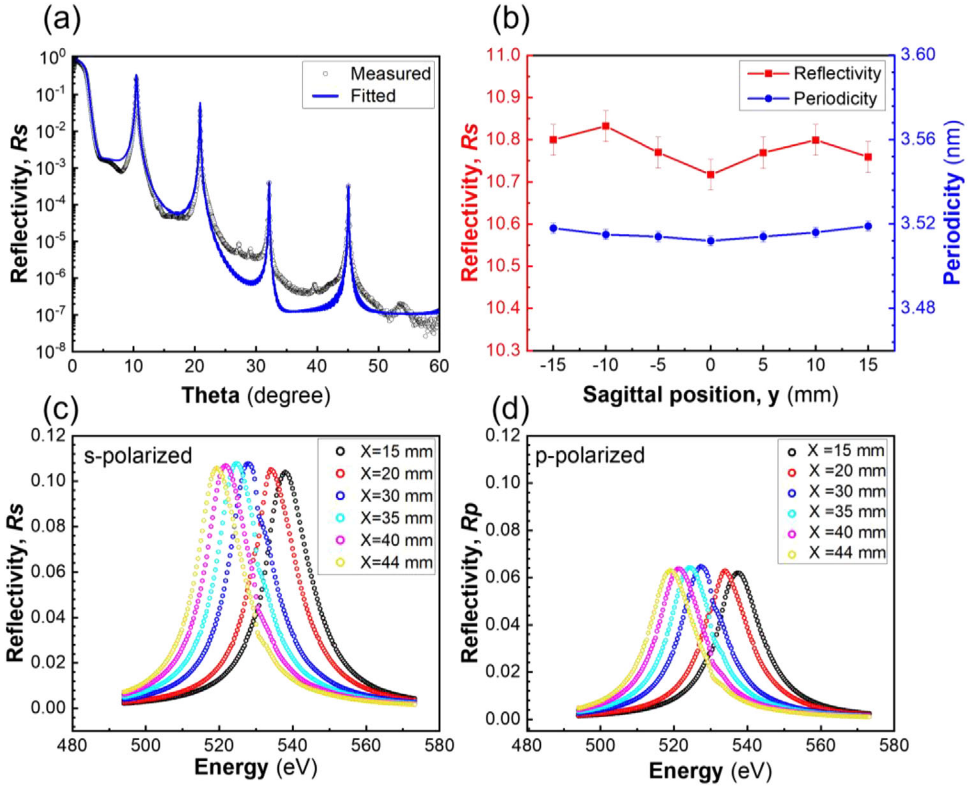

FIGURE 7 | (a) Measured (black circles) and fitted (blue solid line) reflectivity (Rs) profile of the laterally graded multilayer at 1000 eV using s-polarized X-rays, taken at the center of the mirror. (b) Peak reflectivity (red line) and periodicity (blue line) measured at various positions along the sagittal direction (Y-axis) over a 29 mm range at the lateral center. Reflectivity as a function of energy around the O-K edge using (c) s-polarized X-ray, and (d) p-polarized X-ray. Both scans are performed at a fixed incidence angle of $\theta = 20°$.

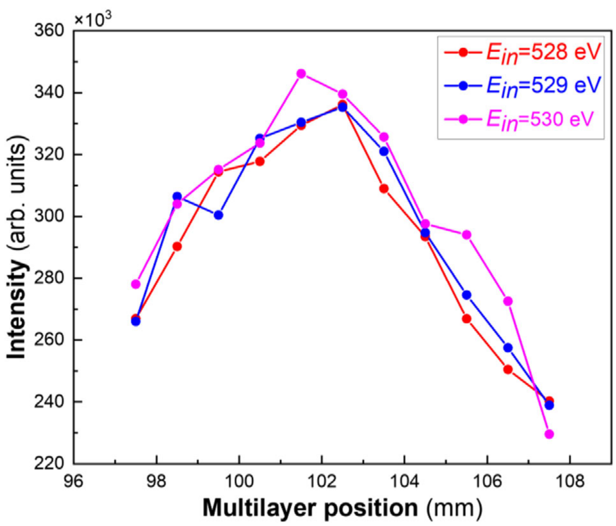

FIGURE 8 | Integrated intensity of the elastic scattering signal as a function of the multilayer's vertical position, demonstrating the spatial dependence of reflectivity due to the lateral grading of the multilayer structure. Peak reflectivity values measured at incident photon energies, E_{in} = 528, 529, and 530 eV are consistent, highlighting the multilayer's tunability and its efficiency in energy-selective polarization analysis.

scattered by an amorphous carbon sample. As illustrated in Figure 8, the integrated intensity of the elastically scattered photons is plotted as a function of the multilayer's vertical position, which corresponds to different positions along the graded periodicity profile. The multilayer was specifically designed with a periodicity gradient tailored to match the energy dispersion of the outgoing X-rays, which are diffracted by the spherical grating. The peak reflectivity values at various incoming photon energies (E_{in} = 528, 529, 530 eV), demonstrating that, when the multilayer is properly positioned, the maximum reflectivity remains nearly constant. This consistency across different energies confirms the effectiveness of the multilayer design in achieving energy-selective polarization analysis without significant loss in reflectivity.

Since the multilayer operates at a grazing angle that deviates from the exact Brewster's angle, the reflected RIXS signal contains a mixture of s- and p-polarized components rather than being purely polarized. As a result, the outgoing spectra represents a partial polarization state.

Figure 9 presents the elastic scattering peaks recorded for both s-polarized light (Figure 9a) and p-polarized light (Figure 9b), measured under two different detection conditions: with the multilayer polarizer inserted in the beam path i.e. reflection mode (shown in blue for s and black for p), and without the polarizer, i.e., in direct detection mode (shown in red for s and orange for p). These measurements were performed to evaluate the efficiency of the multilayer polarizer in distinguishing polarization states of the soft X-ray beam. The reflectivity of the multilayer polarizer was quantitatively assessed by calculating the ratio of the

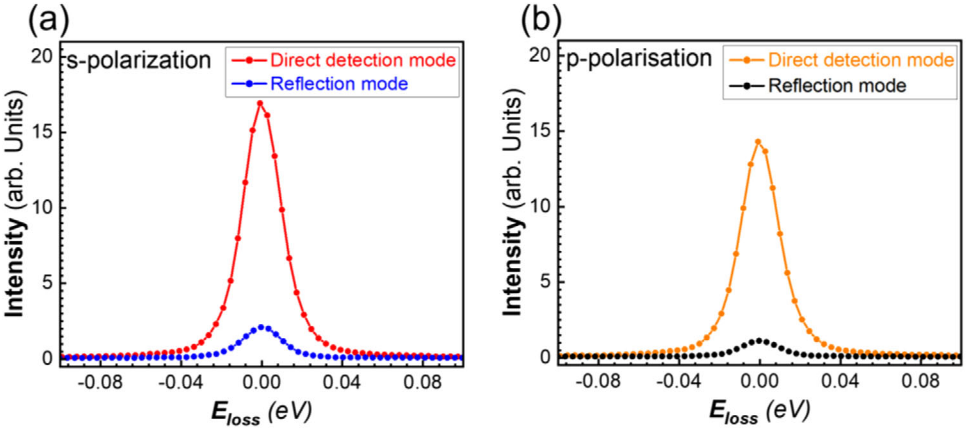

FIGURE 9 | Elastic scattering signal from a carbon tape sample measured using both direct detection and reflection mode for (a) s-polarized light and (b) p-polarized light. Comparison illustrates the effect of the multilayer analyzer on polarization-resolved measurements.

integrated area under the elastic scattering peak obtained in the reflection detection mode to that in the direct detection mode. Based on this analysis, the reflectivity is measured to be ∼ 11.81% for s-polarized light and 7.17% for p-polarized light. These values closely match the anticipated optical performance (Figure 7c,d) for soft X-rays at the BESSY-II Optics beamline, providing further confirmation of the design and measurement.

These values indicate the differential response of the multilayer to the polarization state of incoming X-rays and demonstrate its capability to function as an effective polarization analyzer in soft X-ray scattering experiments.

Building upon the successful demonstration of linear gradient multilayers for polarization analysis, our fabrication capabilities have been further extended to encompass more sophisticated gradient designs for advanced X-ray optical applications. A particularly advanced implementation is the variable gradient laterally graded multilayer, where the multilayer period does not change linearly, but instead follows a controlled, non-uniform gradient across the substrate surface. This design offers enhanced spectral tuning capabilities, enabling optimization for complex beam geometries i.e., Kirkpatrick-Baez (K-B) optics configuration. The fabrication of variable gradient laterally graded multilayers is more challenging than that of constant gradient multilayers because the d-spacing needs to be precisely controlled at specific substrate positions to achieve the desired focusing properties. To address this, the source profile (e.g., W and B_4C) are used to calculate layer thickness, resulting in accurate motor speed profiles that in combination with optimized PID parameters, enable accurate deposition control.

Using the MDS at DLS, a W/B_4C laterally graded multilayer with a spatially variable gradient has been successfully fabricated, demonstrating precise control over the layer structure across the substrate. The multilayer was intentionally designed with an elliptical profile, where the p and q parameters (defined in Equation (2)) are 144.6 m and 0.043 m, respectively, optimized for operating at 10 keV ($\theta = 0.825°$). The multilayer period varies across a 70 mm lateral span, ranging from 5.80 nm at one edge to 1.86 nm at the opposite edge. The lateral gradient is from 0.037 to 0.112 nm/mm. Figure 10 presents both the design target and

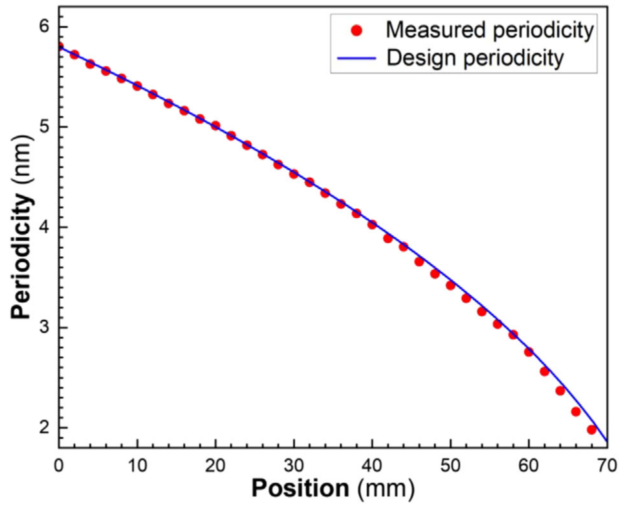

FIGURE 10 | Designed (blue solid line) and measured (red solid square dot) periodicity profile along a gradient direction over 70 mm. The periodicity range spans from 5.79 to 1.85 nm.

the experimentally measured variation in multilayer periodicity, clearly illustrating the successful fabrication of the desired gradient profile. The development of this variable-gradient laterally graded multilayer marks a significant advancement in multilayer optics, enabling precise spatial tuning of optical properties. This innovation greatly enhances the versatility of reflective components used in advanced X-ray and soft X-ray instrumentation, particularly in applications requiring spatially resolved or tunable optical performance.

4 | Conclusion

This study successfully demonstrates the advanced capabilities of the MDS at DLS in fabricating high precision laterally graded multilayer X-ray optics tailored for synchrotron applications. The adjustable mask design is shown to not only enhance the sagittal uniformity but also reduce the time-consuming during optimization. As a result, W/B_4C multilayer polarizer with a well-defined constant lateral gradient of 0.005 nm/mm and low surface roughness of 0.29 nm was developed, highlighting the system's control over nanoscale interface quality. To ensure high optical performance, sagittal thickness uniformity was optimized using an adjustable mask design strategy, achieving excellent uniformity with thickness variation limited to 0.3–0.4% across an 80 mm substrate length.

Comprehensive testing using soft X-rays confirmed the optical quality and polarization selectivity of the fabricated multilayers. The successful integration and operation of the multilayer polarizer on the state-of-the-art I21 RIXS beamline at DLS further validates its functionality and practical integration into high-precision spectroscopic setups. In addition, the MDS demonstrated its versatility by enabling the fabrication of laterally graded multilayer optics with variable gradient from 0.037 to 0.112 nm/mm, which are essential for applications such as variable-angle Bragg reflectors in focusing optics. In summary, this work establishes the MDS as a robust platform for advancing custom multilayer X-ray optics, supporting the growing demands of cutting-edge synchrotron research.

Acknowledgements

This work has been carried out with the support of Diamond Light Source Ltd, UK. The authors would like to acknowledge Adam Howell, Andy Male, and Andrew Malandain from Diamond for their professional support for this project. W.S. acknowledges the Royal Thai Government scholarship for funding.

Conflicts of Interest

The authors declare no conflicts of interest.

Data Availability Statement

The data that support the findings of this study are available from the corresponding author upon reasonable request.

References

1. H. Ni, Q. Huang, Y. Shi, et al., "Development of Large-Size Multilayer Mirrors With a Linear Deposition Facility for X-Ray Applications," *Optical Engineering* 58 (2019): 104105.

2. R. Conley, B. Shi, M. Erdmann, et al., "APS Deposition Facility Upgrades and Future Plans," *ProcSPIE* 9207 (2014): 92070I, https://doi.org/10.1117/12.2062427.

3. C. Morawe, K. Friedrich, M. Osterhoff, and J. C. Peffen, "The New ESRF Multilayer Facility: Progress and Perspectives," *AIP Conference Proceedings* 1234 (2010): 720–723, https://doi.org/10.1063/1.3463311.

4. H. Wang, A. Majhi, W. J. Tan, W. Singhapong, C. Morawe, and K. Sawhney, "Development of an Advanced In-Line Multilayer Deposition System at Diamond Light Source," *Journal of Synchrotron Radiation* 31 (2024): 1050–1057, https://doi.org/10.1107/S1600577524006854.

5. E. Nazaretski, H. Yan, K. Lauer, et al., "Design and Performance of an X-Ray Scanning Microscope at the Hard X-Ray Nanoprobe Beamline of NSLS-II," *Journal of Synchrotron Radiation* 24 (2017): 1113–1119, https://doi.org/10.1107/S1600577517011183.

6. A. G. Buzanich, M. Radtke, U. Reinholz, H. Riesemeier, and F. Emmerling, "Time- and Spatial-Resolved XAFS Spectroscopy in a Single Shot: New Analytical Possibilities for In Situ Material Characterization," *Journal of Synchrotron Radiation* 23 (2016): 769–776, https://doi.org/10.1107/S1600577516003969.

7. N. B. Brookes, F. Yakhou-Harris, K. Kummer, et al., "The Beamline ID32 at the ESRF for Soft X-Ray High Energy Resolution Resonant Inelastic X-Ray Scattering and Polarisation Dependent X-Ray Absorption Spectroscopy," *Nuclear Instruments and Methods in Physics Research A* 903 (2018): 175–192, https://doi.org/10.1016/j.nima.2018.07.001.

8. N. P. Cowieson, C. J. C. Edwards-Gayle, and K. Inoue, "Beamline B21: High-Throughput Small-Angle X-Ray Scattering at Diamond Light Source," *Journal of Synchrotron Radiation* 27 (2020): 1438–1446, https://doi.org/10.1107/S1600577520009960.

9. J. Chen, J. Zhu, M. Cui, et al., "Broadband multilayer polarizers at the energy range of 50–1000 eV," *ProcSPIE* 11032 (2019): 110320Q, https://doi.org/10.1117/12.2520832.

10. M. G. Honnicke, J. W. Keister, and R. Conley, "Synchrotron X-Ray Tests of an L-Shaped Laterally Graded Multilayer Mirror for the Analyzer System of the Ultra-High-Resolution IXS Spectrometer at NSLS-II," *Journal of Synchrotron Radiation* 18 (2011): 862–870, https://doi.org/10.1107/S0909049511031098.

11. C. Morawe, O. Hignette, P. Cloetens, et al., "Graded multilayers for focusing hard X rays below 50 nm," *ProcSPIE* 6317 (2006): 63170F, https://doi.org/10.1117/12.679039.

12. S. Atwal, P. Sarkar, K. Bhattacharyya, et al., "Improvement of High Energy X-Ray Optical Performance of W/Si Supermirror by Optimizing Interface Compounds Using Ultra-Thin Buffer Layer," *Applied Surface Science* 657 (2024): 159736, https://doi.org/10.1016/j.apsusc.2024.159736.

13. F. Eriksson, N. Ghafoor, S. Broekhuijsen, G. Greczynski, N. Schell, and J. Birch, "Morphology Control in Ni/Ti Multilayer Neutron Mirrors by Ion-Assisted Interface Engineering and B 4 C Incorporation," *Optical Materials Express* 13 (2023): 1424–1439, https://doi.org/10.1364/OME.476713.

14. M. Störmer, H. Gabrisch, C. Horstmann, et al., "Ultra-Precision Fabrication of 500 Mm Long and Laterally Graded Ru/C Multilayer Mirrors for X-Ray Light Sources," *Review of Scientific Instruments* 87 (2016): 051804.

15. C. Morawe and M. Osterhoff, "Curved Graded Multilayers for X-Ray Nano-Focusing Optics," *Nuclear Instruments and Methods in Physics Research A* 616 (2010): 98–104, https://doi.org/10.1016/j.nima.2009.11.064.

16. R. Yan, M. Li, and Q. Hou, "Preparation and Testing of Laterally Graded Multilayer with a Double Genetic Algorithm and Root Mean Square Error Optimization in Differential Deposition," *Optics Express* 31 (2023): 22954–22963, https://doi.org/10.1364/OE.486643.

17. C. Morawe, "Graded Multilayers for Synchrotron Optics," *Aip Conference Proceedings* 879 (2007): 764–769, https://doi.org/10.1063/1.2436173.

18. J. Cesar da Silva, A. Pacureanu, Y. Yang, et al., "Efficient Concentration of High-Energy X-Rays for Diffraction-Limited Imaging Resolution," *Optica* 4 (2017): 492–495, https://doi.org/10.1364/OPTICA.4.000492.

19. C. Morawe, "Multilayer Based X-Ray Optics at the ESRF," *Aip Conference Proceedings* 2054 (2019): 060002, https://doi.org/10.1063/1.5084633.

20. H. Wang, S. S. Dhesi, and F. Maccherozzi, "High-Precision Soft X-Ray Polarimeter at Diamond Light Source," *Review of Scientific Instruments* 82 (2011): 123301, https://doi.org/10.1063/1.3665928.

21. H. Wang, S. S. Dhesi, F. Maccherozzi, and K. J. S. Sawhney, "Complete Polarization Analysis of High Energy Soft X-Rays by Combining a Multilayer Phase Retarder with Crystal Analyzer," *Journal of Applied Physics* 111 (2012): 123117, https://doi.org/10.1063/1.4730899.

22. M. A. MacDonald, F. Schäfers, and A. Gaupp, "A Single W/B_4C Transmission Multilayer for Polarization Analysis of Soft X-Rays up to 1 keV," *Optics Express* 17 (2009): 23290–23298, https://doi.org/10.1364/OE.17.023290.

23. M. Cui, L. Sun, J. Zhu, et al., "The Soft X-Ray Polarimeter and Applications at BSRF," *Aip Conference Proceedings* 1234 (2010): 641–644, https://doi.org/10.1063/1.3463288.

24. C. Morawe, J. C. Peffen, R. Supruangnet, et al., "Graded multilayers for fully polarization resolved resonant inelastic x-ray scattering in the soft x-ray range," *ProcSPIE* 9207 (2014): 92070J, https://doi.org/10.1117/12.2061827.

25. J. Zhu and M. Cui, in *Ellipsometry*, ed. W. Faustino (IntechOpen, 2017).

26. K.-J. Zhou, A. Walters, and M. Garcia-Fernandez, "I21: An Advanced High-Resolution Resonant Inelastic X-Ray Scattering Beamline at Diamond Light Source," *Journal of Synchrotron Radiation* 29 (2022): 563–580, https://doi.org/10.1107/S1600577522000601.

27. R. Conley, C. Liu, C. M. Kewish, A. T. Macrander, and C. Morawe, "Multilayer growth in the APS rotary deposition system," *ProcSPIE* 6705 (2007): 670505, https://doi.org/10.1117/12.736024.

28. C. Morawe and J.-C. Peffen *ProcSPIE* 7448 (2009): 74480H.

29. S. Chen, J. Sun, J. Li, et al., "Controlling Lateral Thickness Distributions of Magnetron Sputtering Deposited Coatings Using Shadow Masks," *Optical Materials Express* 14 (2024): 101, https://doi.org/10.1364/OME.500104.

30. H. Huang, Y. Feng, J. Yu, R. Qi, and Z. Wang, "The Fabrication of a High-Precision Rotational Symmetric Hyperboloid Mirror by Magnetron Sputtering with Film Thickness Correction," *Coatings* 12 (2022), https://doi.org/10.3390/coatings12081055.

31. X. Liu, Z. Zhang, H. Song, et al., "Comparative Study on Microstructure of Mo/Si Multilayers Deposited on Large Curved Mirror with and without the Shadow Mask," *Micromachines* 14 (2023), https://doi.org/10.3390/mi14030526.

32. Z. Zhang, R. Qi, Y. Yao, et al., "Improving Thickness Uniformity of Mo/Si Multilayers on Curved Spherical Substrates by a Masking Technique," *Coatings* 9 (2019), https://doi.org/10.3390/coatings9120851.

33. R. P. Borase, D. K. Maghade, S. Y. Sondkar, and S. N. Pawar, "A Review of PID Control, Tuning Methods and Applications," *International Journal of Dynamics and Control* 9 (2021): 818–827, https://doi.org/10.1007/s40435-020-00665-4.

34. D. L. Windt, "Reduction of stress and roughness by reactive sputtering in W/B4C multilayer films," *ProcSPIE* 6688 (2007): 66880R, https://doi.org/10.1117/12.730647.

35. D. L. Windt, "IMD—Software for Modeling the Optical Properties of Multilayer Films," *Computers in Physics* 12 (1998): 360–370, https://doi.org/10.1063/1.168689.

36. M. Bjorck and G. Andersson, "GenX: An Extensible X-Ray Reflectivity Refinement Program Utilizing Differential Evolution," *Journal of Applied Crystallography* 40 (2007): 1174–1178, https://doi.org/10.1107/S0021889807045086.

37. A. Sokolov, P. Bischoff, and F. Eggenstein, "At-Wavelength Metrology Facility for Soft X-Ray Reflection Optics," *Review of Scientific Instruments* 87 (2016): 052005, https://doi.org/10.1063/1.4950731.

38. A. Sokolov, M. G. Sertsu, A. Gaupp, M. Luttecke, and F. Schafers, "Efficient High-Order Suppression System for a Metrology Beamline," *Journal of Synchrotron Radiation* 25 (2018): 100–107, https://doi.org/10.1107/S1600577517016800.

39. W. Singhapong, A. Majhi, W. J. Tan, et al., "Development of High-Performance Multilayer Monochromators," *Advanced Optical Materials* (2025): 01312, https://doi.org/10.1002/adom.202501312.

40. P. N. Rao, V. Srihari, P. Rajput, S. N. Jha, T. Ganguli, and S. K. Rai, "Investigation of Long Term Stability of W/B_4C Multilayer Structures," *Thin Solid Films* 755 (2022): 139327, https://doi.org/10.1016/j.tsf.2022.139327.

41. Y. A. Vainer, A. E. Pestov, K. A. Prokhorov, et al., "Analysis of Cross-Correlation of Interface Roughness in Multilayer Structures With Ultrashort Periods," *Journal of Experimental and Theoretical Physics* 103 (2006): 346–353, https://doi.org/10.1134/S1063776106090020.

42. C. C. Walton, G. Thomas, and J. B. Kortright, "X-ray Optical Multilayers: Microstructure Limits on Reflectivity at Ultra-Short Periods," *Acta Materialia* 46 (1998): 3767–3775, https://doi.org/10.1016/S1359-6454(98)00083-4.

43. A. Jafari, D. D. M. Ferreira, S. Kadkhodazadeh, et al., "Long-Term Performance and Durability of Ir/B4C Multilayer X-Ray Mirrors: Focusing on Composition, Structure, and Reflectivity Properties," *Journal of Astronomical Telescopes, Instruments, and Systems* 6 (2020): 034005, https://doi.org/10.1117/1.JATIS.6.3.034005.

44. S. Massahi, F. E. Christensen, and D. D. M. Ferreira, "Investigation of Boron Carbide and Iridium Thin Films, an Enabling Technology for Future X-Ray Telescopes," *Applied Optics* 59 (2020): 10902, https://doi.org/10.1364/AO.409453.